Publication Year	2021
Acceptance in OA	2023-02-01T13:23:19Z
Title	Modeling and measurement of the scattering properties of the source pinhole in the BEaTriX facility
Authors	SPIGA, Daniele, SALMASO, Bianca, BASSO, Stefano
Handle	http://hdl.handle.net/20.500.12386/33101
Volume	INAF-OAB internal report 2021/04

Advanced Telescope for High-Energy Astrophysics (*ATHENA*)

BEaTriX, the Beam Expander Testing X-ray facility

Modeling and measurement of the scattering properties of the source pinhole in the BEaTriX facility

INAF/OAB technical report 04/2021

Issued by ***D. Spiga***, ***B. Salmaso***, ***S. Basso*** (INAF/OAB)

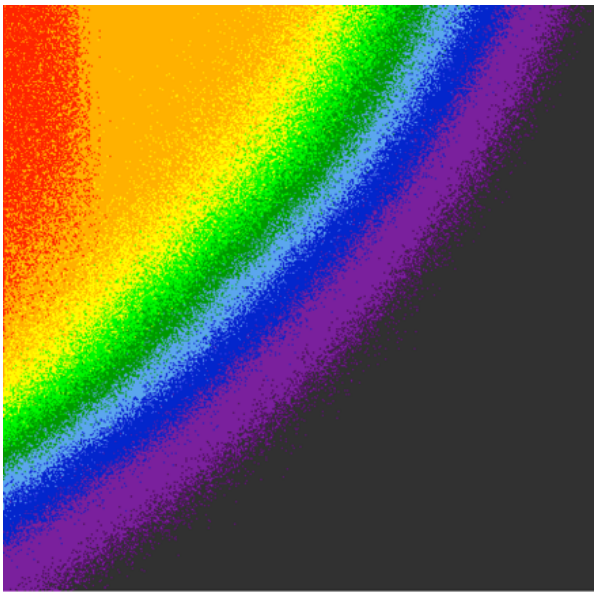

Istituto Nazionale di Astrofisica (INAF)

Via del Parco Mellini, 00100 Roma, Italy

Osservatorio Astronomico di Brera (OAB)

Via Brera 28, 20121 Milano, Italy

Via E. Bianchi 46, 23807 Merate, Italy

1. Scope of the document

The purpose of this brief technical note is to provide an assessment of the performance of the tungsten pinhole placed in front of the microfocus Incoatec X-ray source with Titanium anode in the BEaTriX X-ray facility. The pinhole is a part of the collimator kit by Amptek purchased years ago to collimate a solid-state detector, and consists of a small (1/2 inch) tungsten disk with a 2.2 mm thickness and a 450 µm diameter. The pinhole is placed at a 20 mm distance from the source and limits the beam along the short arm of the facility, avoiding so the X-ray incidence on the tube walls which might cause unwanted X-ray reflection/scattering or diffuse background. At the same time, the pinhole located near the X-ray source provides visual reference for the parabolic mirror alignment.

Pinholes are crucial optical components, as they have to diaphragm an X-ray beam without degrading it. Due to the closeness of the lateral walls of the pinhole to the X-rays, the surface has to be properly ruggedized in order to avoid unwanted reflections or diffuse scattering when X-rays impinge on it in grazing incidence conditions. Should this condition not be fulfilled, the pinhole would cause a broadening of the X-ray source and a consequent worsening of the finally collimated X-ray beam in BEaTriX. In this short note, we will show measurements of the X-ray beam in the BEaTriX facility aiming at ascertaining the scattering properties of the pinhole surface. The conclusion is that the amount of scattered/reflected radiation off the pinhole is hardly detectable and that the pinhole appears perfectly suitable for the collimation of the X-ray beam in the short arm of BEaTriX.

2. Simulation and modelling

The behavior of the X-ray source in BEaTriX through the pinhole has been modelled by means of a dedicated X-ray program in IDL language. The X-ray source is a 2D Gaussian profile with a 35 µm FWHM as per the characterization performed in the *Incoatec GmbH* factory (Figure 1).

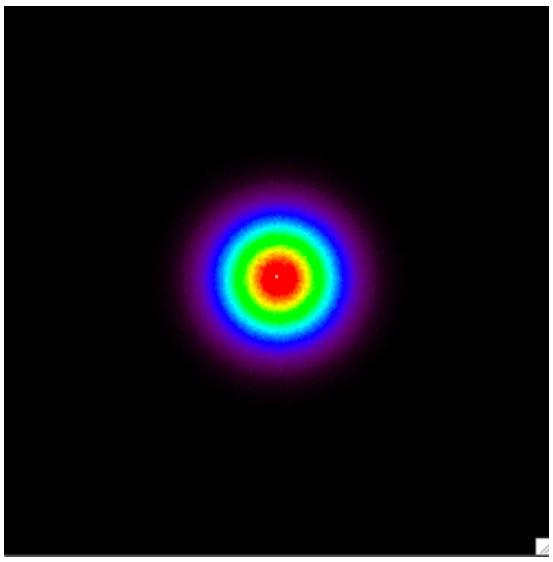

Figure 1: modelling the Incoatec X-ray source as a 2D gaussian source with a 35 µm FWHM.

We have now simulated the beam passing through the pinhole with the geometric parameters described in Sect. 1, initially with zero thickness aiming at checking the simulation correctness. The pinhole is itself much wider than the X-ray source and the beam is diverging in all the directions; hence, placing a CCD in front of the beam emerging from the pinhole we expect the photons to trace a disc with a blurred contour, due to both the small but finite extent of the X-ray source and the scattering properties of the pinhole wall.

The CCD is placed at a 6031 mm distance from the X-ray source, on the vacuum flange that will be used to mount the wavefront sensor. At this distance, the circle has a diameter of approx. 135 mm and so is too wide to be entirely detected by the CCD, which has a 27.6 mm side. Nevertheless, the source-pinhole system can be tilted and rotated in order to have the disc edge to fall within the field of the CCD, near its center (Figure 2).

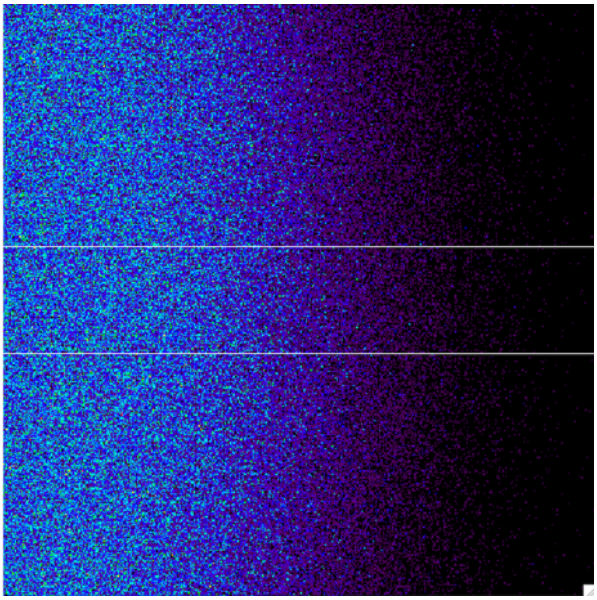

Figure 2: the right edge of the disc, as simulated in the CCD field (binning 4x4), assuming the inner surface of the pinhole of zero length. The edge diffuseness is purely due to the finite extent of the X-ray source. The central rectangle encloses the region selected for the intensity profile to be analyzed.

The illumination near the disc edge fades to zero gradually due to the finite source size, which is in turn related to the fading abruptness. If one takes the central 5 mm stripe in Figure 2 and integrating along columns, the intensity profile matches well a gaussian integral, as expected. The model adopted for fitting it is

$$y_{fit}(x) = N \int_0^x e^{-\frac{(x\prime - c)^2}{2w^2}} dx'$$

with N, c, w degrees of freedom, and taking x as the horizontal coordinate on the CCD in mm. The w parameter expresses the edge width rms: a simple proportion $w' = 2.354 \cdot w \cdot d/D$ ($d = 20$ mm, $D = 6031$ mm) easily returns the FWHM of the X-ray source, w'; in this case we correctly obtain $w' \approx 35$ µm (Figure 3), as per the factory characterization.

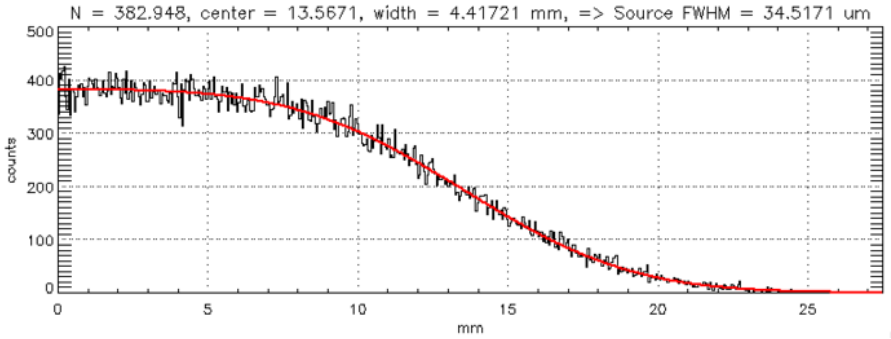

Figure 3: the profile intensity from the simulation in Figure 2, along with a gaussian integral fit. The AMOEBA routine in IDL has been used to achieve the computation.

We now take the pinhole length to the real value a 2.2 mm, and suppose the inner surface specular reflecting, assuming the tungsten reflectivity variable with the X-ray energy (< 20 keV) and the incidence angle (near 0.54 deg): the disc then increases a few mm in size, and the light-dark transition becomes broader also. If we keep the same gaussian fitting model, then the apparent source size increases by a few microns (Figure 4). It is interesting to note that, if the pinhole has a cylindrical shape, the specular reflected component that gets superimposed to the geometric transition on a given angle of the disc edge actually comes from the *other side of the pinhole* (with a radial lag equal to the pinhole diameter, Figure 5).

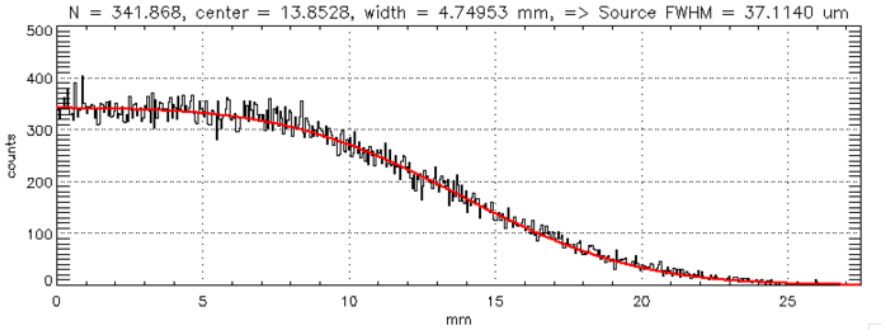

Figure 4: pinhole 2.2 mm long, with the ideal reflectivity of tungsten, specular reflective walls.

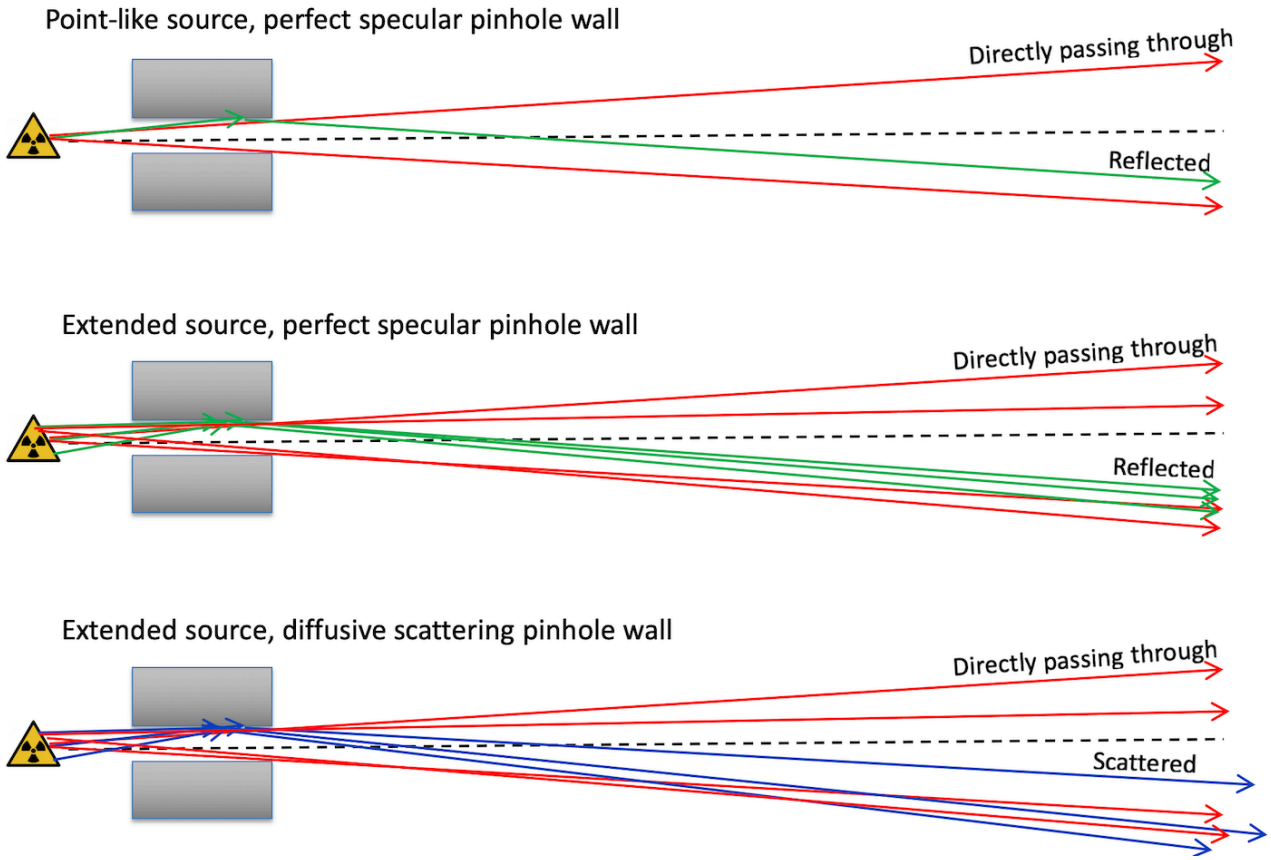

Figure 5: the three different scattering models considered; a) reflected rays end close to the opposite edge of the disc; b) an extended source creates a diffuse edge with both direct and reflected component; c) diffuse scattering adds further diffuseness in the light-dark transition.

We now assume that the inner surface of the pinhole be also scattering at angles ϑ, centered on the specular direction, and determined by a typical Lorentian distribution;

$$P(\theta) = \frac{\Omega}{\pi(\theta^2 + \Omega^2)}$$

There is no way to know *a priori* what the real angular distribution of scattered X-rays is, but this is usually an effective description. The distribution is symmetric, peaked at ϑ=0, normalized over ϑ from -∞ to +∞, and finally Ω equals ½ FWHM and the ½ HEW. In the simulation, the generation of the n-th deviation angle according to this distribution is obtained altering the orientation of the normal unit vector to the inner surface of the pinhole, in the incidence angle, according to the formula:

$$\theta_n = \Omega \tan\left(\frac{\pi}{2} r_n\right)$$

where r_n is a random number between -1 e +1 in a uniform distribution. We can now adopt the following descriptive model in the presence of diffuse scattering:

$$y_{fit}(x) = N_1 \int_0^x e^{-\frac{(x\prime - c_1)^2}{2w^2}} dx' + N_2 \left[e^{-\frac{(x-c_2)^2}{2w^2}}\right] \otimes \left[\frac{1}{(x/D)^2 + \Omega^2}\right]$$

taking as fit parameters: N_1, N_2, c_1, c_2, and Ω (some constants were embedded in N_2). The convolution between the gaussian profile and the Lorentzian allows us keeping into account the edge broadening due to the finite source extent and the reflective scattering. The presence of the c_2 term is due to part of the gaussian beam being reflected inwards, rather than ending on the edge of the geometric shadow.

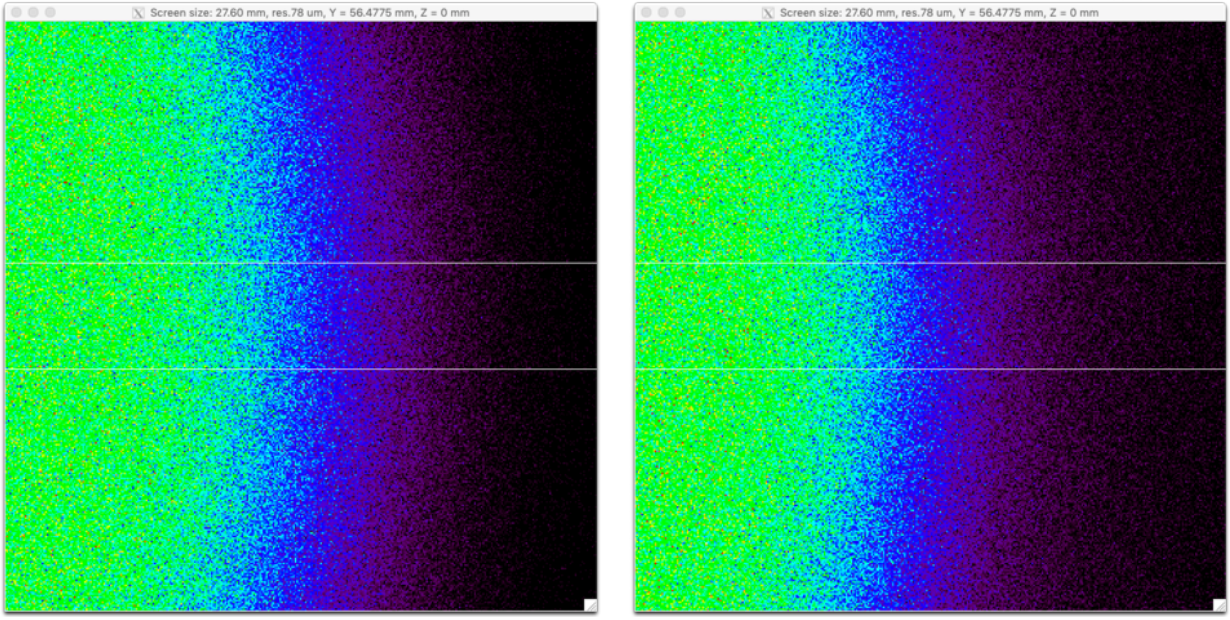

Figure 6: simulating the illumination edge with reflective/diffusive surface of the pinhole, with (left) Ω = 0° and (right) Ω = 0.1°.

Running the fit using the AMOEBA routine in IDL returns Figure 6 and the intensity profile is fitted in Figure 7; the 2nd term center is located at +5 mm (blue marker in Figure 7) while the direct beam center is the green marker. However, in order to have stable values in the parameter, 50 million rays have to be

launched. With the new model, the source FWHM gets close to the one of the source collimated by a non-reflecting pinhole (Figure 3), and the scattering FWHM fitted from the distribution also increases with Ω.

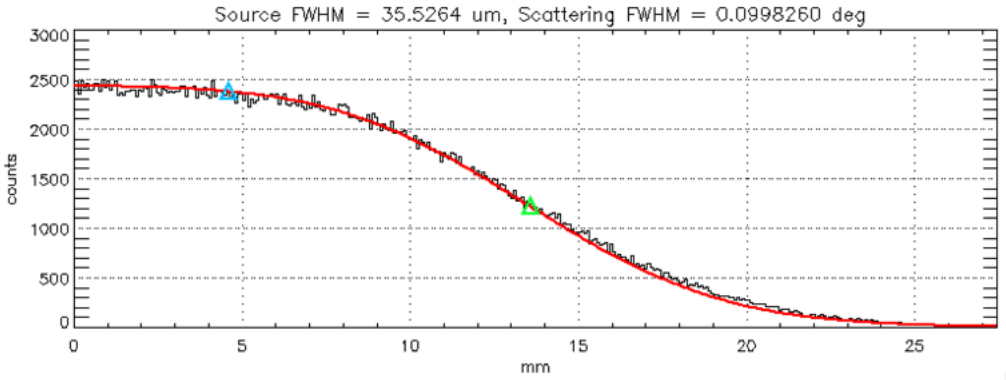

Figure 7: pinhole 2.2 mm thick, Tungsten reflectivity from 0.5 to 20 keV, Ω = 0.1 deg. The red line represents the best fit of the simulated distribution using the convolution model.

The determination of the Ω parameter from fitting the intensity profile is relevant to assessing the level of expected contamination with scattered rays within the mirror entrance slit in BEaTriX. For example, simulation shows that a non-reflecting surface or a specular (non-diffusive) surface would not pose any problems, whereas a Ω = 0.1 deg parameter value would deviate a significant number of rays in the slit aperture (Figure 8).

We finally mention that the pinhole is not exactly cylindrical: the profile is probably conical converging with a 0.65 deg slope. This would be helpful to increase the deviation of reflected/scattered rays outwards and far from the directly passing beam; hence, the simulations shown here are probably pessimistic.

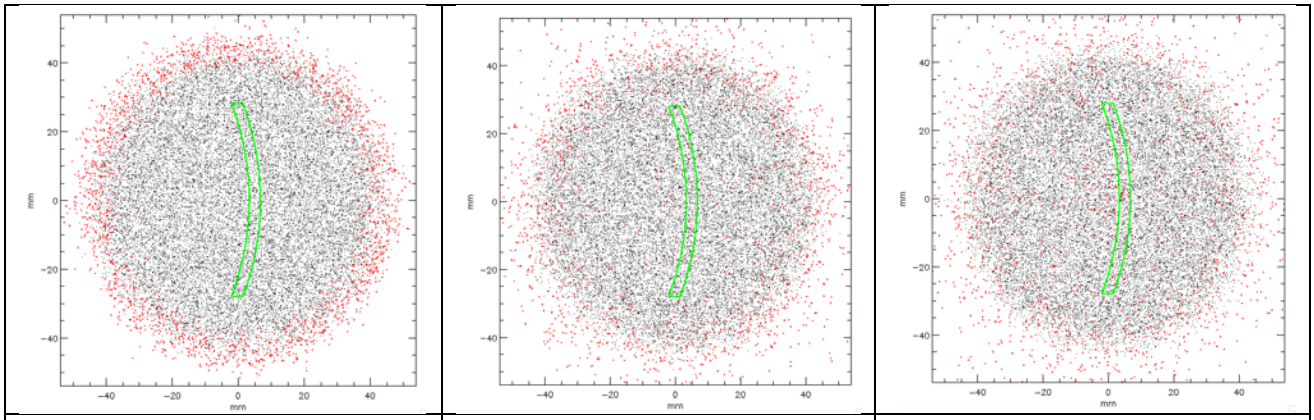

Ω = 0°	Ω = 0.1°	Ω = 0.2°

Figure 8: direct beam distribution (black dots) and reflected/diffuse rays (red dots) at the distance of the parabola entrance slit, for variable values of the scattering parameter. The entrance slit is traced in green.

3. Measurements and summary

The beam emerging from the pinhole was characterized experimentally, changing the orientation with respect to the CCD camera Andor iKon L SO mounted in a fixed location on the optical chamber of BEaTriX. Different sectors of the beam could be recorded near its edge. The source was set at 30 kV, 150 μA, and each exposure was 60 s. The exposures are shown in Figure 9.

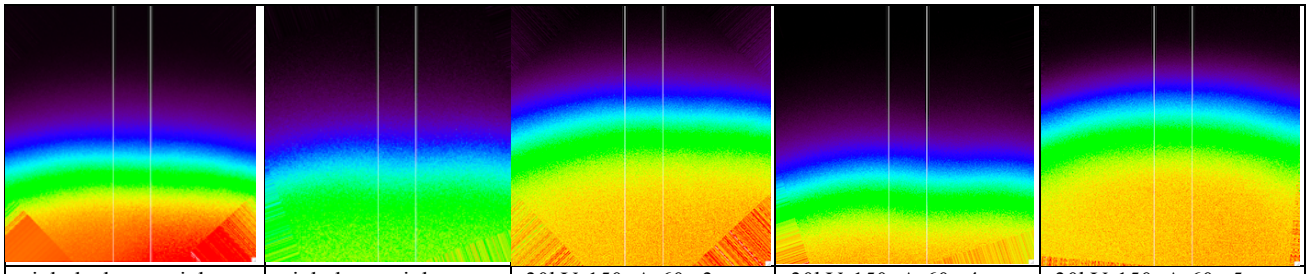

pinhole_bottomright	pinhole_topright	30kV-150uA-60s-3	30kV-150uA-60s-4	30kV-150uA-60s-5

*Figure 9: measured exposures near the edge of the illumination disc. Images **have been rotated** to have the illumination gradient lie in radial direction. The corners are rotation artifacts, not affecting the analysis.*

File name	Source FWHM	Reflectivity	Scattering FWHM
20210601-pinhole_bottomright	35.4 µm	1×10^{-5}	0.003 deg
20210601-pinhole_topright	38.8 µm	1×10^{-4}	0.009 deg
20210629-30kV-150uA-60s-3	36.7 µm	4×10^{-6}	0.010 deg
20210629-30kV-150uA-60s-4	35.8 µm	8×10^{-6}	0.017 deg
20210629-30kV-150uA-60s-5	34.0 µm	3×10^{-5}	0.004 deg

Table 1: results of the analysis/fit of the intensity gradients from the measured exposures.

After an appropriate rotation aimed at aligning the intensity gradient in vertical direction, we have extracted the intensity profile in the central 300-pixel stripe. The application of the fitting routine performs as shown in Figure 10. All the best-fit parameter sets are consistent with the values listed in Table 1. We note, remarkably, that the source FWHM is very close to its nominal value, with some fluctuations that might depend on the imperfect source symmetry or some imperfection in the pinhole axis misalignment. The pinhole surface reflectivity fits an extremely low value (< 0.0001) denoting pinhole walls sufficiently ruggedized to avoid significant reflection. The scattering FWHM parameter, finally, fits a peaked distribution of scattered rays; nevertheless, due to the extremely low reflectivity/scattering level, i.e. the normalization of the Lorentzian function, this parameter becomes mostly meaningless.

The conclusion of this characterization in X-rays is that the pinhole in use is suitable for BEaTriX activity, as the amount of scattered radiation seems negligible, and that the source size inferred from the intensity gradient near the edge of the diverging beam is fully consistent with the value expected from the specifications.

20210601-pinhole_bottomright	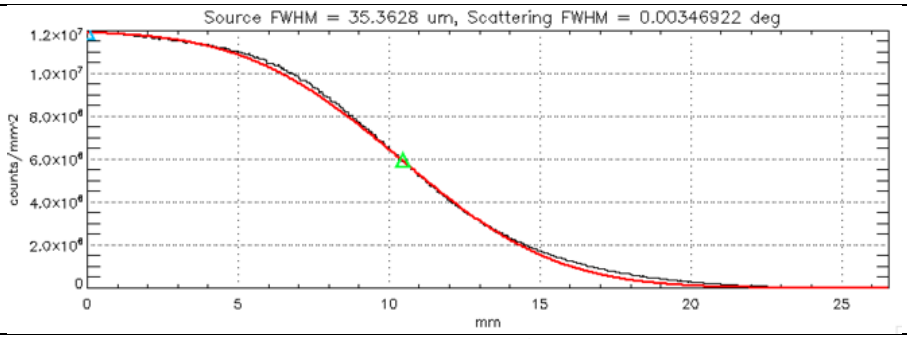
20210601-pinhole_topright	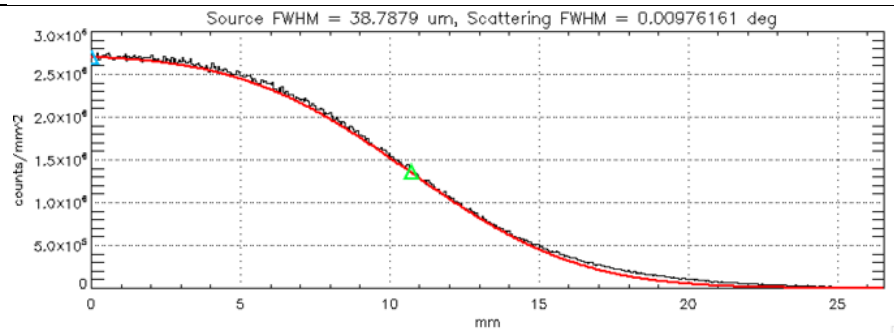
20210629-30kV-150uA-60s-3	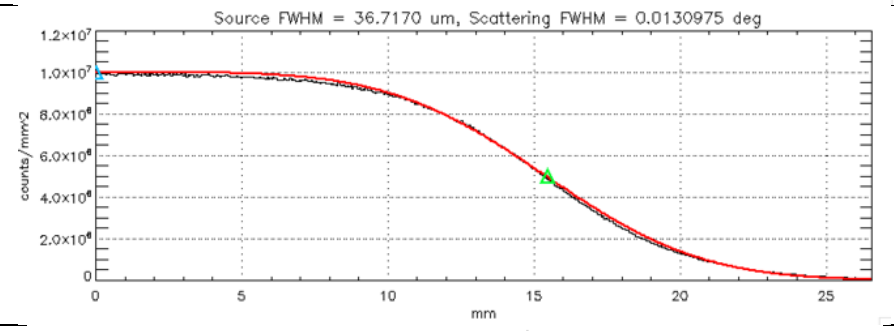
20210629-30kV-150uA-60s-4	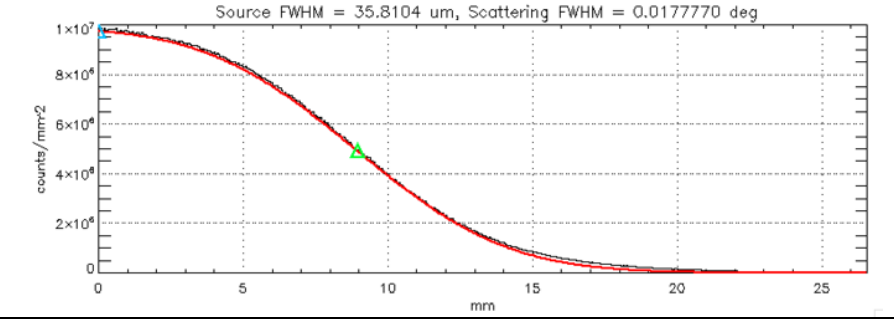

20210629-30kV-150uA-60s-5	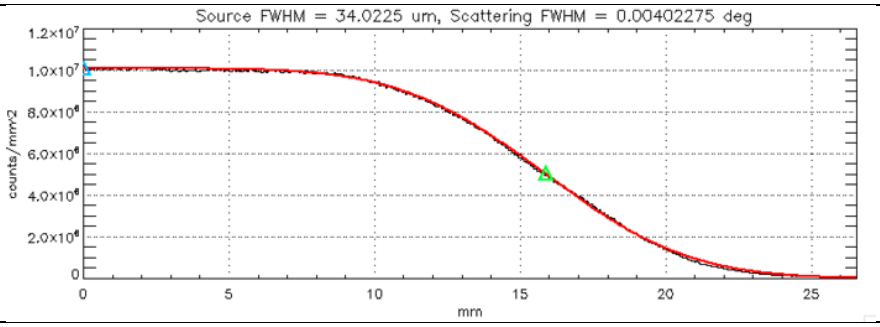

Figure 10: fitting the radial sections of the beam with the convolution model.